Cerebral Cortex, 2021;00: 1–15

https://doi.org/10.1093/cercor/bhab330
Original Article

ORIGINAL ARTICLE

Verbal and General IQ Associate with Supragranular Layer Thickness and Cell Properties of the Left Temporal Cortex

D. B. Heyer[1,†], R. Wilbers[1,†], A. A. Galakhova[1], E. Hartsema[1], S. Braak[1], S. Hunt[1], M. B. Verhoog[1,2], M. L. Muijtjens[1], E. J. Mertens[1], S. Idema[3], J. C. Baayen[3], P. de Witt Hamer[3], M. Klein[4], M. McGraw[5], E. S. Lein[5], C. P. J. de Kock[1], H. D. Mansvelder[1,‡] and N. A. Goriounova[1,‡]

[1]Department of Integrative Neurophysiology, Amsterdam Neuroscience, Center for Neurogenomics and Cognitive Research (CNCR), Vrije Universiteit Amsterdam, Amsterdam 1081HV, The Netherlands, [2]Department of Human Biology, Neuroscience Institute, University of Cape Town, Cape Town 7925, South Africa, [3]Department of Neurosurgery, Amsterdam UMC, location VUmc, Vrije Universiteit Amsterdam, Amsterdam 1081HV, The Netherlands, [4]Department of Medical Psychology, Amsterdam UMC, location VUmc, Vrije Universiteit Amsterdam, Amsterdam 1081HZ, The Netherlands and [5]Allen Institute for Brain Science, Seattle, WA 98109, USA

Address correspondence to email: n.a.goriounova@vu.nl; h.d.mansvelder@vu.nl
[†]D. B. Heyer and R. Wilbers have equal contribution
[‡]H. D. Mansvelder and N. A. Goriounova, senior authors

Abstract

The left temporal lobe is an integral part of the language system and its cortical structure and function associate with general intelligence. However, whether cortical laminar architecture and cellular properties of this brain area relate to verbal intelligence is unknown. Here, we addressed this using histological analysis and cellular recordings of neurosurgically resected temporal cortex in combination with presurgical IQ scores. We find that subjects with higher general and verbal IQ scores have thicker left (but not right) temporal cortex (Brodmann area 21, BA21). The increased thickness is due to the selective increase in layers 2 and 3 thickness, accompanied by lower neuron densities, and larger dendrites and cell body size of pyramidal neurons in these layers. Furthermore, these neurons sustain faster action potential kinetics, which improves information processing. Our results indicate that verbal mental ability associates with selective adaptations of supragranular layers and their cellular micro-architecture and function in left, but not right temporal cortex.

Key words: action potential, dendrites, human neurons, intelligence, language

Introduction

Our world is built around expressing ourselves through spoken and written language, and verbal intelligence is a major contributor to general cognitive ability (Deary et al. 2010). General intelligence is a strong predictor not only of successful education and career, but also of socio-economic status, lifestyle choices, health, and longevity (Amunts et al. 1999; Strenze 2007). However, large differences in cognitive ability exist between individuals that are likely to persist throughout their lifetime, as intelligence is a highly stable (Deary et al. 2013) and heritable (Coleman et al. 2019) trait. The underlying neurobiological basis for these individual differences is poorly understood.

Human intelligence is supported by a selection of distributed regions of the neocortex. This network was first described by Jung and Haier as Parieto-Frontal Integration Theory (P-FIT), and includes the dorsolateral prefrontal cortex, the inferior and superior parietal lobule, the anterior cingulate and regions within occipital lobes and the temporal lobe, including BA21 (Jung and Haier 2007). In this network, the cognitively salient information is proposed to flow from brain regions within the temporal and occipital lobes, critical to early processing of sensory information, and is then fed forward to the parietal cortex, that interacts with frontal regions. Many of these areas implicated in intelligence—especially temporal lobe areas such as BA21—show predominantly left-hemispheric associations (Jung and Haier 2007), suggesting a dominant role of the left hemisphere in processing of cognitive information. Larger volume, thicker cortex, and cortical activation patterns in frontal and temporal areas were shown to associate with higher IQ scores (Haier et al. 2004; McDaniel 2005; Colom et al. 2006; Choi et al. 2008; Colom et al. 2009; Karama et al. 2009; Deary et al. 2010). In contrast, cortical thinning of frontal and temporal lobes was shown to associate with dementia, cognitive impairment, and several other psychiatric disorders (Du et al. 2007; Patel et al. 2021). The correlations between cortical thickness and total and verbal intelligence are especially strong in the left temporal lobe (Jung and Haier 2007; Choi et al. 2008; Colom et al. 2009; Deary et al. 2010). These findings are consistent with the function of the left temporal lobe in integrating semantic information from distinct brain regions and its role in concept retrieval (Binder et al. 2009). This specialization of the left temporal cortex for verbal expression is supported by multiple studies in split-brain patients, patients with lesions and brain imaging data from healthy subjects (Damasio et al. 2004; Gazzaniga 2005; Gainotti 2006). Thus, any relationship of cortical microstructure with verbal intelligence would most likely reveal itself in the left temporal lobe.

Cortical function ultimately depends on the activation of neuronal circuits with laminar organization (Self et al. 2019), where different layers are engaged at different timepoints of the cognitive tasks reflecting the information flow and top-down attention. The architecture of this laminar structure shows large interindividual variation in human cortical language areas (Amunts et al. 1999, 2003; Uylings et al. 2005). Such interindividual variability in microscopic structure may reflect differences in cognitive ability between individuals. As cortical layers contain stereotypically organized microcircuits of neurons, the observed differences could arise from changes in the function and structure of these neurons. Indeed, not only cortical thickness, but also the underlying dendritic structure and function of pyramidal neurons in temporal cortex associate with total IQ scores (Goriounova et al. 2018).

Supragranular cortical layers 2 and 3 (L2/L3) in humans have a disproportionately high volume compared to primates and other mammalian species (Hutsler et al. 2005), and hold principal neurons with extensive dendritic trees that are thought to be the main source of rich cortico-cortical projections (Douglas and Martin 2004). Whether individual variation in fine structure of laminar organization and specifically of L2/L3 in temporal cortex can explain differences in verbal intelligence between individuals is not known. Here, we address this issue by testing how cortical microstructure and neuronal properties of the left temporal cortex (middle temporal gyrus, MTG, Brodmann area 21, BA21) associate with verbal intelligence.

Although the MTG by itself is not essential for speech (is not part of classical Broca and Wernicke areas), several lines of evidence point to this region as an important site in verbal cognition. Analysis of localized lesions, functional imaging and positron emission tomography in large cohorts of subjects identified this region as a part of the semantic system serving concept and word retrieval and categorization (Damasio et al. 2004; Binder et al. 2009). Furthermore, multiple studies of patients with lesions in MTG show that this area is strongly associated with language comprehension and specific semantic deficits (Hart and Gordon 1990; Hillis and Caramazza 1991; Chertkow et al. 1997; Dronkers et al. 2004). In addition, recordings of single neuron activity in awake neurosurgery patients performing verbal tasks show that MTG is the area of temporal cortex where neurons selectively respond to language and verbal memory tasks (Ojemann et al. 1988, 2002).

Because of this role of the left MTG (BA21) as an integral part of the semantic processing network that underlies verbal cognition, we collected Verbal IQ scores (VIQ) as well as Full Scale (FSIQ) and Performance IQ scores (PIQ) from Wechsler Adult Intelligence Scale (WAIS IV) tests that subjects underwent shortly before surgery. Based on the reported correlations between cortical thickness of BA21 and intelligence (Jung and Haier 2007; Choi et al. 2008; Colom et al. 2009; Deary et al. 2010), we hypothesized that this increase in cortical thickness in subjects with higher verbal IQ is reflected in the changes of cortical microstructure of the left-hemispheric area BA21—specifically in the density, composition, and volume of the upper cortical layers as they are involved in cortico-cortical processing of information.

Methods

Human Subjects and Brain Tissue

All procedures were approved by the Medical Ethical Committee of the VU University Medical Center, and in accordance with the declaration of Helsinki and Dutch license procedures. All subjects provided written informed consent for the use of data and tissue for scientific research. All data were anonymized.

Human cortical brain tissue was resected during neurosurgery in order to gain access to deeper pathological brain structures, typically hippocampus, or amygdala. In all patients, the cortical tissue originated from middle temporal gyrus (MTG, Brodmann area 21) and was resected as a block of cortical tissue (1–1.5 cm in diameter) from the middle part of MTG, at 4 cm from the anterior pole. Functional mapping was used to prevent the resection of speech areas. Subjects underwent surgery for the treatment of mesial temporal sclerosis, removal of hippocampal tumor, low-grade hippocampal lesion, cavernoma,

or otherwise unspecified medial temporal lobe pathology. Non-pathological cortical tissue was obtained from 59 subjects (28 males, 31 females; age 18–66 years; 26 left hemisphere and 33 right hemisphere resections, Supplementary Table 1). Cortical thickness was measured in 91 slices from 36 of these subjects. From 25 subjects, full morphological reconstructions of 71 neurons were obtained. Action potentials were recorded in 149 neurons from 35 subjects.

In all subjects, the resected neocortical tissue was not part of the epileptic focus or tumor and was removed to access deeper lying structures. The non-pathological status of tissue was based on the surgeon's assessment, pre-surgical MRI scans and the histological assessment of tissue slices after DAPI, DAB, and/or NeuN staining (the integrity of layer structure, absence of abnormal cells, or gliosis). We and others (Molnár et al. 2008; Wang et al. 2015; Hodge et al. 2019) have repeatedly demonstrated that using access tissue samples, one can study non-pathological properties of human circuits (Testa-Silva et al. 2010, 2014; Verhoog et al. 2016; Goriounova et al. 2018; Obermayer et al. 2018; Kroon et al. 2019). We observed no correlations of cellular parameters or cognitive scores with the subject's disease history and age (Supplementary Table 3). All anatomical, morphological and physiological data were collected and analyzed while blind to the subjects' IQ scores.

All primary data analyses were performed blind to the cognitive tests scores of the subjects. These analyses include extraction of cortical thickness from MRI, histological staining, layer thickness quantification, cell body size and density measurements, cell body diameter measurement from biocytin stained neurons, morphological reconstructions of dendritic structure, and action potential feature extraction from electrophysiological recordings. All statistics reported in the study were performed by researchers who were not involved in the primary data analysis or IQ quantification.

IQ Scores

Full Scale IQ (FSIQ; for 58 subjects), verbal IQ (VIQ; for 50 subjects), and performance IQ (PIQ; for 51 subjects) scores were obtained using the Dutch version of the Wechsler Adult Intelligence Scale-III (WAIS-III) or WAIS-IV (Supplementary Table 2). The tests were typically administered within a short time before surgery as part of a neuropsychological examination. Cognitive tests were performed in the clinical setting and quantified by the clinical neuropsychologists as part of the diagnostic procedure prior to surgery. The IQ scores are calculated based on performance on the following subtests: vocabulary, similarities, information, comprehension, arithmetic, digit span, and letter-number sequencing for VIQ; picture completion, block design, matrix reasoning, digit symbol-coding, and symbol search for PIQ. For FSIQ, performance on all subtests is aggregated.

Slice Preparation

Immediately after surgical resection, the cortical tissue was transferred to carbogenated ice-cold artificial cerebrospinal fluid (aCSF) containing (in mM): 110 choline chloride; 26 $NaHCO_3$; 10 D-glucose; 11.6 sodium ascorbate; 7 $MgCl_2$; 3.1 sodium pyruvate; 2.5 KCl; 1.25 NaH_2PO_4; and 0.5 $CaCl_2$ (300 mOsm) and transported to the laboratory. The time between resection of the tissue and the start of preparing slices was less than 15 min. After manual removal of the pia 350-µm-thick cortical slices were prepared in the same ice-cold solution used for transport and described above. After slicing, the slices were transferred to holding chambers filled with aCSF, containing (in mM): 125 NaCl; 3 KCl; 1.2 NaH_2PO_4; 1 $MgSO_4$; 2 $CaCl_2$; 26 $NaHCO_3$; 10 D-glucose (300 mOsm), and bubbled with carbogen gas (95% O_2/5% CO_2). The slices were stored in the holding chambers for 30 min at 34 °C, and at least 30 min at room temperature prior to recordings.

Electrophysiological Recordings

Cortical slices were placed in a recording chamber with a continuous flow of oxygenated aCSF. All experiments were performed at 32–35 °C. Infrared differential interference microscopy (IR-DIC; BX51WI microscope, Olympus) was used to visualize neurons within the slices. Patch pipettes (3–5 MOhms) were filled with intracellular solution (ICS) containing (in mM): 110 K-gluconate; 10 KCl; 10 HEPES; 10 K-phosphocreatine; 4 ATP-Mg; 0.4 GTP; pH adjusted to 7.3 with KOH; 285–290 mOsm; 5 mg/mL biocytin. After establishing whole cell configuration, membrane potential responses to depolarizing current injection steps (30–50 pA step size) were recorded. Recordings were sampled at frequencies of 10–50 kHz and low-pass filtered at 10–30 kHz using Multiclamp 700A/B amplifiers (Axon Instruments). Recordings were digitized with an Axon Digidata 1440A, acquired with pClamp software (Axon) and later analyzed offline using custom-written scripts in MATLAB (R2019b, Mathworks).

Morphological Analysis

Cells were loaded with (0.5%) biocytin present in the ICS during electrophysiological recordings. Afterwards, the slices were fixed in paraformaldehyde (PFA, 4%) and the recorded cells were stained with the chromogen 3,3-diaminobenzidine tetrahydrochloride (DAB) using the avidin-biotin-peroxidase method. Next, the slices were mounted on glass microscope slides and embedded in mowiol underneath a glass coverslip. Successfully stained neurons with clear cell body contours were used for cell body diameter quantification. The cell bodies were imaged using Surveyor Software (Chromaphor, Oberhausen, Germany) with a ×100 oil objective. These images were analyzed in ImageJ. The soma diameter was measured as the maximum distance from side to side at the base of the cell body, as a line perpendicular to the direction of apical dendrite. A sub-selection of these biocytin-stained neurons was selected for dendritic reconstruction. This selection was based on uniform biocytin signal, presence of complete dendrites without obvious slicing artifacts, and apical dendrite reaching to layer 1. These selected neurons were digitally reconstructed using Neurolucida software (Microbrightfield) and a 100× oil objective (Olympus). After reconstruction, morphologies were checked for accurate reconstruction in x/y/z planes for presence of unconnected, missed, or incompletely reconstructed dendrites. Finally, reconstructions were crosschecked by an independent researcher for false-positive/false-negative dendrites using an overlay in Adobe Illustrator between the Neurolucida reconstruction and Z-stack projection image from Surveyor Software (Chromaphor, Oberhausen, Germany), as reported previously in (Mohan et al. 2015).

L2/L3 pyramidal neurons were identified based on morphological and electrophysiological properties, somatic depth and position within layers from DAPI-stained slices. The morphological reconstructions for these cells that passed the quality control were then used to extract the total dendritic length (TDL) and number of branches on basal dendrites.

Cortical Thickness Measurements

To determine cortical thickness, the fixated cortical slices that were previously recorded from, were stained with 4′,6-diamidino-2-phenylindole (DAPI) and remounted. The intensity of the fluorescence is an indication of the density of cell bodies within the cortical slice. This allowed us to differentiate the different cortical layers. Normal light and fluorescent images were taken using NeuroExplorer software (Microbrightfield). The outlines of cortical layers were tracked in ImageJ software. The cortical thickness and layer thickness were measured along radially drawn lines, parallel to fiber tracks, apical dendrites and blood vessels visible in the tissue. The lines were drawn by an independent experienced researcher to minimize errors and bias. Since no clear distinction can be made with DAPI between layers 2 and 3, and between layers 5 and 6, we treated L2/L3 and L5/L6 as single regions in the analysis. Cortical thickness varies between gyri and sulci in the cortex. Therefore, we only measured cortical thickness in the gyral crown. Cortical slices that did not clearly contain gyral crown were excluded. Cortical slices that were cut at an angle to the pia-white matter axis were identified by slicing artifacts and unclear borders between cortical layers and excluded from the analysis.

MRI Scans and Cortical Thickness Analysis

T1-weighted brain images (1 mm thickness) were acquired with a 3 T MR system (Signa HDXt, General Electric, Milwaukee, Wisconsin) as a part of pre-surgical assessment, the scans were analyzed using the Freesurfer image analysis suite (http://freesurfer.net) (Fischl and Dale 2000), previously reported in (Goriounova et al. 2018). Calculation of the cortical thickness was done as the closest distance from the gray/white boundary to the gray/CSF boundary at each vertex and was based both on intensity and continuity information from the entire three-dimensional MR volume. Neuroanatomical labels were automatically assigned to brain areas based on Destrieux cortical atlas parcellation as described in (Fischl 2004). Middle temporal gyrus was selected based on Destrieux cortical atlas parcellation in the hemisphere where the resected tissue originated. Cortical thickness at each vertex in this selected area was averaged for each subject.

Cortical Microstructure Analysis from NeuN Stained Slices

Several slices (1–3 per subject) were fixed in paraformaldehyde (PFA, 4%) for 48 h, transferred to phosphate buffer solution PBS + sodium azide. Slices were then cryoprotected in 30% sucrose, frozen and re-sectioned at 30 µm using a sliding microtome (Leica SM2000R). Tissue slices were stained using the Biocare Intellipath FLX slide staining automated platform. All NeuN tissue sections were pre-mounted onto gelatin-coated slides, the day prior to IHC staining and first allowed to dry flat for 30–60 min, then were briefly rinsed in Milli-Q water. All slides were placed in 37 °C oven overnight prior to IHC staining the following day. At the day of staining, slides were peroxidase blocked in Bipocare 1X TBS wash buffer (Biocare # TWA945M), endogenous peroxidase activity was blocked using 3% hydrogen peroxidase in 1× TBS wash buffer. All slides underwent Heat Induced Epitope Retreival (HIER) methods, in 98 °C Sodium Citrate buffer, pH 6.0 for 20 min, then allowed to cool at room temperature for 20 min. Next, slides were rinsed in Milli-Q water and equilibrated using 1× TBS buffer, loaded onto the Biocare intelliPath FLX Slide Stainer and incubated on intelliPath Staining Platform using the following conditions: incubation for 10 min in intelliPath Background Punisher (Biocare# IP974G20), then application of 0.5 µg/mL (1:2000) of NeuN mouse primary antibody (clone A60, Millipore- MAB377) in Biocare Renaissance Background Reducing Diluent (Biocare #PD950L) for 75 min. Next, tissue sections were rinsed in 1× TBS wash buffer and treated with BiocareMouse Secondary reagent (Mach4 kit [IPK5011 G80]) for 10 min, then washed in 1× TBS buffer, followed by incubation in iBiocare Universal HRP Tertiary reagent (#IPK5011 G80) for 15 min then rinsed in 1× TBS wash buffer. All sections were developed using a mixture of Chromogen IP FLX DAB (IPK5011 G80) and Biocare DAB Sparkle (Biocare # DS830M) applied for 1 min. Upon autostainer run completion, all slides were unloaded into Milli-Q water, dehydrated through a series of graded alcohols, cleared in Formula 83, and coverslipped with DPX for final detection of stained neurons.

Subsequently, the images of stained subsections were acquired with 20x air on Aperio microscope at a resolution of 1 µm to 1 pixel. The quantification of cell densities and cell body sizes was performed from the acquired subsections images by using custom-made MATLAB scripts (R2019b, Mathworks). Within each subsection, regions of interest (ROIs) were selected manually covering the whole slice. The border between L1 and L2 was visually identified as a characteristic sharp increase in cell body size and density, L3–L4 border was identified at the transition from large L3 cells to 3-fold smaller L4 cell bodies. Each ROI was selected as a trapezoid with bases along the border between L1 and L2 (upper base, 500–700 µm in length), the border between L3 and L4 (lower base, 500–700 µm in lengths) and the sides parallel to the apical dendrites. The L2/L3 thickness was calculated for each ROI separately (mean length of the sides) and each ROI was split in four sublayers (L2, L3a, L3b, and L3c defined as 25% of the L2/L3 thickness). The cell densities were calculated as a number of cells in the 1 mm^3 volume of tissue. The volume was defined as the product of selected ROI area (for each sublayer) and 25 µm optical thickness of tissue subsection (tissue subsection thickness of 30 µm corrected for the poor visibility and detection of deeper lying cells within the subsection). We validated MATLAB scripts by manually quantifying neuronal parameters from ROIs from 15 slices, the manual quantification was similar to the automated quantification (average cell density quantified manually $27\,010 \pm 3592$ neurons/mm^3, quantified with MATLAB scripts $26\,595 \pm 4649$ neurons/mm^3). The obtained neuronal density are very similar to previously reported for human cortex (layer IIIa: 20964 ± 2709 neurons/per mm^3, average of all cortical layers: 24186 neurons/per mm^3 reported in (DeFelipe et al. 2002)).

Statistical Analysis

Statistical significance of relationships between parameters was determined using linear regression. Since multiple cells or slices were measured per subject, parameters were first averaged per subject before statistical testing. Differences between groups were tested for significance using the non-parametric two-sided Mann–Whitney *U* test. Corrections for multiple testing were performed according to the Benjamini-Hochberg false discovery rate procedure. All statistical analysis was performed using Matlab (R2019a, Mathworks). Partial correlations controlling for the effects of age and gender were computed using SPSS 26 (IBM).

Data Availability

Source data are provided with this paper. To protect the privacy of the subjects in this study, subject numbers have been randomized in Supplementary Tables 1 and 2, and the source data for Supplementary Table 3 and Supplementary Figure 4 are only available upon request from the corresponding author (NAG).

Code Availability

All customized Matlab scripts used for physiological feature extraction are available at https://github.com/INF-Rene/Morphys.

Results

IQ Scores Associate with Thickness of L2/L3

Verbal intelligence has been shown to have strong structural correlates in the brain, including a prominently larger cortical thickness exclusively in the left temporal lobe of subjects with higher VIQ scores (Choi et al. 2008). However, it is not known whether this difference is due to the upscaling of all cortical layers or only a selective set of layers. To investigate this, we collected neurosurgically resected left or right MTG tissue from 59 subjects treated for epilepsy or tumor (Supplementary Table 1). The resected tissue was not part of the epileptic focus or tumor, but was resected to gain access to the focus or tumor (see methods). On average, total cortical thickness, as well as L2/L3 thickness, was larger in the right MTG than left MTG. This observed asymmetry reflects a natural asymmetry in cortical thickness between left and right hemispheres, as evidenced by a recent large analysis of MRI scans of >17 000 healthy individuals from 99 datasets, where middle temporal area was shown to have higher thickness in the right hemisphere than in the left (Kong et al. 2018). We first asked whether dimensions of specific cortical layers in left or right MTG associate with IQ scores. To visualize cortical layer boundaries, we DAPI stained cortical sections and quantified the thickness of the cortical layers at 4 to 5 locations from multiple (range = 1–9, median = 2) slices per subject (Fig. 1*a*,*b*). To minimize biological variation, we quantified layer thickness only at the crown of the gyrus (Fig. 1*b*). We calculated average layer thickness per subject and compared 2 groups of subjects with low and high verbal IQ (VIQ) scores. Only in the left and not right MTG, we found that subjects with high VIQ scores (VIQ > 90) have a larger cortical L2/L3 compared to subjects with lower VIQ scores (VIQ < 90), while other layers were similar across the VIQ groups (Fig. 1*c*, data values for individual slices are shown in Supplementary Fig. 1). We also observed a strong positive correlation between individual VIQ scores of the subjects and total cortical thickness and L2/L3 thickness in the left MTG ($R = 0.8$, $R^2 = 0.66$; Fig. 1*d*,*e*, Supplementary Fig. 2). In contrast, VIQ scores did not correlate with the thickness of other cortical layers (Fig. 1*e*, Supplementary Fig. 2), indicating that the larger L2/L3 in subjects with higher verbal intelligence underlies the larger total cortical thickness of the left MTG.

Intellectual performance is generally measured by full scale IQ (FSIQ) scores that are derived from both verbal (VIQ) and non-verbal, performance IQ (PIQ) scores. We analyzed cortical layer thickness separately for VIQ, PIQ and FSIQ in the left and right MTG. The summarized linear regression results for all layers in left and right MTG, and for verbal and performance IQ scores revealed that the correlations of FSIQ, VIQ, and PIQ scores with total cortical thickness are attributable to the selective expansion of L2/L3 in the left MTG. Although FSIQ, VIQ, and PIQ all significantly correlated with total and L2/L3 thickness in the left MTG, the variance explained (R^2) was higher when running linear regression on VIQ than PIQ (Supplementary Fig. 3). To exclude possible confounding effects of age and gender, we calculated partial correlations for the relationship between VIQ and L2/L3 thickness. We computed the zero-order and partial correlation coefficients (r) while controlling for age and gender separately for FSIQ, VIQ and PIQ and L2/L3 thickness in the left MTG. We find that the correlations remained high and statistically significant (Supplementary Fig. 4*a*). Furthermore, L2/L3 thickness did not correlate significantly with age of the subjects and did not show significant difference between males and females (Supplementary Fig. 4*b*,*c*).

Since total cortical thickness and L2/L3 thickness are also correlated with each other ($r = 0.77$, $P < 0.000$), we employed a generalized linear mixed-effects model to determine how much each of these thicknesses predict FSIQ, VIQ, and PIQ when accounting for this correlation. Surprisingly, the model revealed that not the total cortical thickness, but only L2/L3 thickness is a determinant of FSIQ, VIQ, and PIQ. Furthermore, mixed-effects modeling also proved this relationship to be specific to the left hemisphere ($P = 0.90$ for general L2 and L3 effect, $P = 0.009$ for hemisphere: L2/L3 interaction). Thus, subjects with higher general and verbal IQ scores have thicker cortex in the left MTG due to the selective increase in thickness of L2/L3, and it is the thickness of these layers that determines the correlation between IQ and cortical thickness.

As cortical thickness in human subjects is usually measured using structural MRI scans, we next asked whether cortical thickness quantified using histological methods is correlated with cortical thickness quantified from MRI. To this end, we quantified cortical thickness from pre-surgical MRI scans using voxel-based morphometry (Fig. 1*f*). We selected only MTG area in the hemisphere where the resected tissue originated and calculated average MTG cortical thickness for each subject. We tested whether MRI-derived cortical thickness correlated with the histological quantifications of cortical thickness. We find that MRI and histological quantifications positively correlate with each other. Moreover, cortical thickness measured from MRI also positively correlates with the L2/L3 thickness in the gyral crown, the metric that we find most strongly related to verbal intelligence (Fig. 1*f*). Thus, L2/L3 thickness in the left MTG strongly associates with cognitive function, including verbal cognitive function.

Thicker L2/L3 Contains Lower Neuronal Densities and Larger Cells

Next, we asked how the expansion of L2/L3 would affect the overall microstructure of these layers. We hypothesized that a thicker L2/L3 would contain larger neurons that are dispersed over a greater volume to accommodate larger dendritic arbors. To analyze the microstructure of L2/L3, we stained human frontal, temporal, and parietal cortices (left and right hemisphere) with NeuN (neuronal nuclei) antibodies in an independent group of 16 neurosurgery subjects. As L2/L3 thickness shows great variability even within the same slice of the same subject, we measured cell densities and cell size in multiple regions of interest (ROIs) covering the whole slice (24 slices, 113 ROIs). Each ROI was manually selected to include only layers 2 and 3 (Fig. 2*a*). Similar to previously published data (DeFelipe et al. 2002), we find that neuronal density decreases

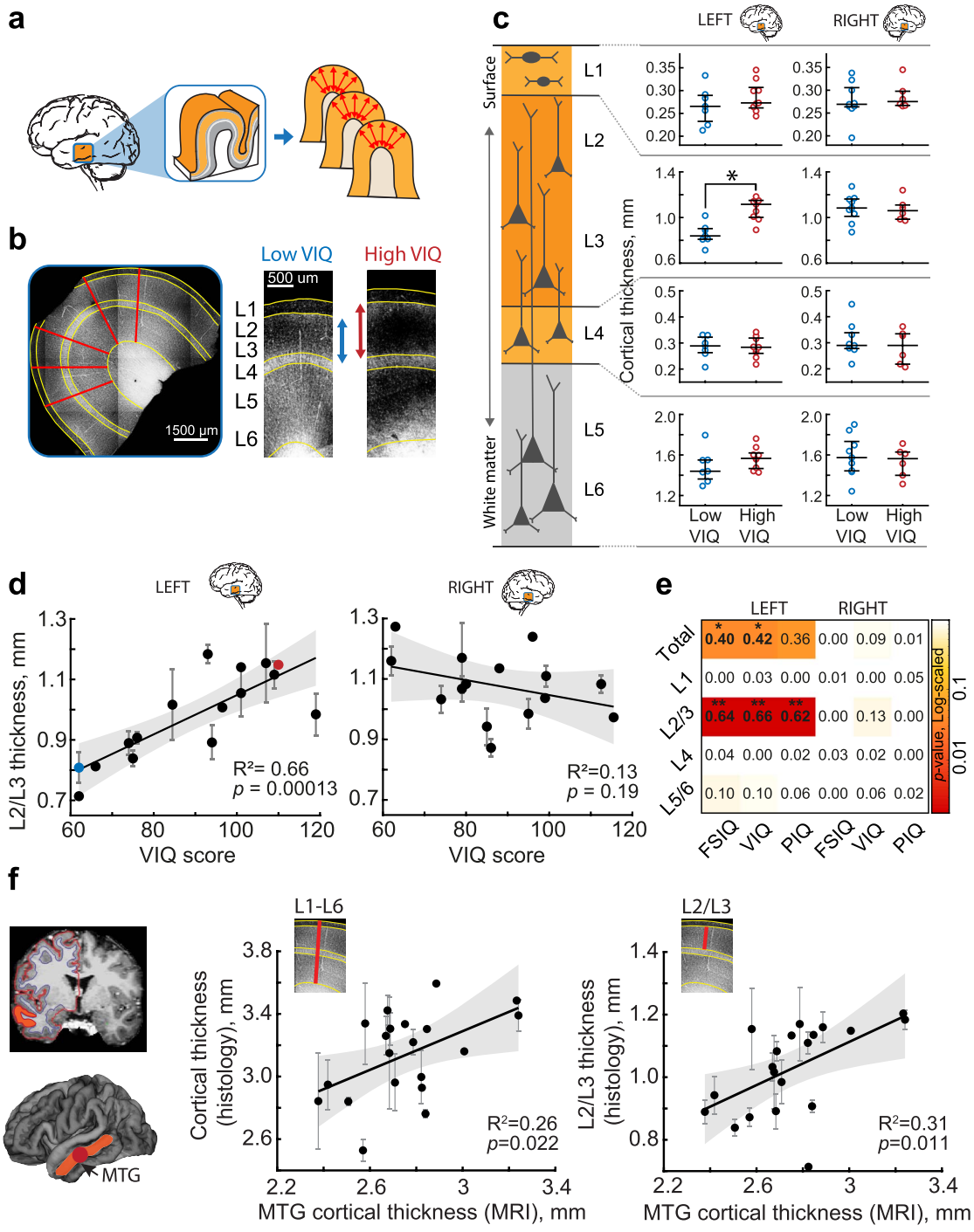

Figure 1. Thickness of cortical L2/L3 in the left MTG is associated with higher VIQ scores. (*a*) Slices from temporal lobe tissue resected during neurosurgery were DAPI-stained and imaged to determine the thickness of the cortical layers. (*b*) Example of cortical thickness measurements: the borders between the cortical layers were drawn on the images (yellow lines). For each patient, the average thickness was calculated along 4–5 radial lines (red) from several slices of gyral crown. (*c*) Subjects with higher VIQ scores have thicker L2/L3 in the left MTG (Median(IQR) = 1.116(1.002–1.150) mm), than subjects with low VIQ (0.839(0.809–0.903) mm, Mann–Whitney *U* test, $U = 32$, $P = 0.0021$). Open circles represent the average thickness of the different cortical layers from each subject (from top to bottom: L1; L2/L3; L4; L5/L6), red for subjects with VIQ > 90, blue for subjects with VIQ < 90. Separately for left (left panel) and right (right panel) hemisphere (Left: low VIQ: n subjects = 7, *n* slices = 13, high VIQ: *n* subjects = 9, *n* slices = 22. Right: low VIQ: *n* subjects = 9, *n* slices = 25, high VIQ: *n* subjects = 6, *n* slices = 16). Here and further: long black horizontal lines are median values; vertical lines are interquartile ranges. (*d*) L2/L3 cortical thickness positively correlates with VIQ in the left (*n* subjects = 16, *n* slices = 35, $F(1,14) = 27.1$), but not in the right MTG (*n* subjects = 15, *n* slices = 41, $F(1,13) = 1.87$). Here and further: error bars indicate SEM, shaded area represents 95% confidence bounds, insets show R^2 and *P*-values. The blue and red data points correspond to the examples shown in *b*. (*e*) Heatmap showing linear regression results (R^2) for all cortical layers, both hemispheres, for Full Scale (FSIQ), verbal (VIQ) and performance (PIQ) IQ test scores. *P*-values are color-coded, $^*P < 0.05$; $^{**}P < 0.01$. (*f*) Cortical thickness in MTG quantified from MRI scans, correlates with the MTG thickness from histological quantifications shown in *c* and *d*. Left panel shows an example of an MRI scan with

from L2 to deeper L3, while the cell body area increases (Fig. 2*b*,*c*). In relation to layer thickness specifically, the neuronal density within sublayers is negatively associated with the average thickness of L2/L3: subjects with thicker L2/L3 had a less densely populated L3, and these correlations were especially strong for deeper L3 (Fig. 2*d*,*e*, Supplementary Fig. 5). In addition, the cell body area positively correlated with the thickness of L2/L3 (Supplementary Fig. 5). These results show that the thicker L2/L3 contain similar counts of neurons in L3, while their cell bodies are larger and more dispersed over a larger volume.

Higher VIQ Associates with Larger Neurons with more Complex Dendrites

Pyramidal cells are the principal computational units of the cortex and integrate information on their large dendrites spanning multiple layers (DeFelipe et al. 2002; Gidon et al. 2020). We asked whether the thicker L2/L3 layers in the left MTG from subjects with higher VIQ also contain larger pyramidal neurons. To this end, we quantified the cell body diameter from the biocytin-filled neurons from L2/L3 in the left and right MTG slices as shown in Figure 1. The neurons from the left MTG in subjects with VIQ >90 had significantly larger cell bodies than those from subjects with lower VIQ, while in the right MTG, the distributions of cell body diameters are similar between subjects with lower and higher VIQ scores. Thus, higher VIQ associates not only with the thicker L2/L3 (Fig. 1), but these layers also contain pyramidal neurons with larger cell bodies in the left MTG (Fig. 3*a*).

We have previously shown that dendritic length and complexity of pyramidal cells positively associates with Full Scale IQ scores (Goriounova et al. 2018). However, it is not known whether left-lateralization of verbal function also applies to the cellular level. To test whether the total dendritic length (TDL) of pyramidal neurons in L2/L3 from the left MTG correlates with VIQ scores, we selected neurons from Figure 3*a* with complete dendritic trees and fully reconstructed pyramidal morphologies from the left and right MTG. In line with our findings on layer thickness and cell body size, we observed a significant positive correlation between VIQ scores and TDL for pyramidal neurons in L2/L3 in the left and not right MTG from these subjects (Fig. 3*c*). Moreover, VIQ scores also correlated with the number of branches on basal dendrites in these neurons (Fig. 3*c*, data values for each neuron are shown in Supplementary Figure 6), indicating that the larger dendrites in the subjects with higher VIQ are also more complex and the observed correlation with TDL is not only due to a longer apical shaft in deeper lying neurons. After controlling for age and gender, TDL also correlated with FSIQ, but not PIQ (Supplementary Fig. 4*a*), showing that neuronal structure in the left MTG is specifically associated with verbal cognition. Furthermore, TDL did not correlate significantly with age of the subjects and was not different between male and female subjects (Supplementary Fig. 4*b*,*c*).

Dendritic length is closely related to the location of the cell soma within cortex and deeper lying cells generally have larger dendrites (Mohan et al. 2015; Kalmbach et al. 2018). As subjects with higher VIQ have thicker total cortex, their pyramidal cells are on average located deeper than those from subjects with lower VIQ (Fig. 3*d*, Supplementary Fig. 7*a*) and individual VIQ scores correlated with neuronal depth (Supplementary Fig. 7*b*). To ensure that the difference in TDL was not simply the result of recording from deeper neurons in high VIQ patients, we corrected neuron depth for total cortical thickness. The relative depth of these cells within the layer was not different (low VIQ median (IQR) = 0.49 (0.30–0.58), high VIQ = 0.62 (0.51–0.79), $P = 0.22$) (Fig. 3*d* right panel) and did not correlate with VIQ scores ($R^2 = 0.31$, $P = 0.097$, Supplementary Fig. 7*b*), indicating that the cells from both groups were recorded at similar relative depths within the layers. Thus, our results show that variation in L2/L3 thickness in the left MTG is accompanied by changes in pyramidal cell dendrite length and complexity in these layers, and both associate with verbal intelligence. Longer and more complex dendrites may endow the pyramidal cells with a larger dendritic surface for forming synaptic connections, and allow separate branches of the dendritic tree to act as independent computational compartments increasing the complexity of information processing (Poirazi et al. 2003; Gidon et al. 2020).

Neurons from Subjects with Higher VIQ Maintain Fast Action Potentials

Dendritic tree size directly influences action potential (AP) firing of pyramidal neurons (Eyal et al. 2014; Goriounova et al. 2018). It speeds up AP kinetics, increases the AP onset rapidity, and allows large pyramidal neurons to better time-lock AP firing to synaptic inputs (Goriounova et al. 2018). Moreover, human pyramidal neurons from subjects with higher Full Scale IQ scores are able to maintain faster rise speeds during sustained firing. As larger TDL in pyramidal neurons from L2/L3 in the left MTG supports higher VIQ, we asked whether these neurons are also able to sustain faster AP kinetics. We performed patch-clamp recordings and recorded action potentials at different instantaneous frequencies and quantified their rise speeds (Fig. 4*a*). We observed similar lateralization towards the left MTG: pyramidal cells in L2/L3 in the left MTG from subjects with higher VIQ scores fired APs with faster rise speeds at 21–40 Hz than those of subjects with lower VIQ. We did not observe any significant differences between VIQ groups in AP rise speeds of neurons from the right MTG (Fig. 4*b*,*c*). Finally, AP rise speeds at 21–40 Hz positively correlated with VIQ in the left, but not in the right MTG (Fig. 4*d*, data values for individual neurons are shown in Supplementary Fig. 6*b*). We checked whether one high value of AP rise speed (marked red in Fig. 4*d*) biased the results. After excluding this data point from the regression analysis, the correlation remained strong and significant ($R^2 = 0.67$, $P = 0.007$). After controlling for age and gender, AP rise speeds also correlated with FSIQ, but not PIQ (Supplementary Fig. 4*a*). Furthermore, AP rise speeds did not correlate significantly with age of the subjects and were not different between male and female subjects (Supplementary Fig. 4*b*,*c*). Thus, subjects with higher VIQ (and FSIQ) have larger pyramidal neurons in L2/L3 of the left MTG that are able to sustain fast action potential (AP) rise speed during high-frequency firing. These findings are in line with

white-gray matter boundaries highlighted with colored lines, MTG is marked orange, the resected area is marked red. MTG cortical thickness from MRI scans of the resected MTG positively correlates with total cortical thickness (middle, n subjects = 20, n slices = 56, $F(1,18) = 6.26$) and L2/L3 thickness (right, n subjects = 20, n slices = 56, $F(1,18) = 8.1$) from histological analysis of the resected MTG.

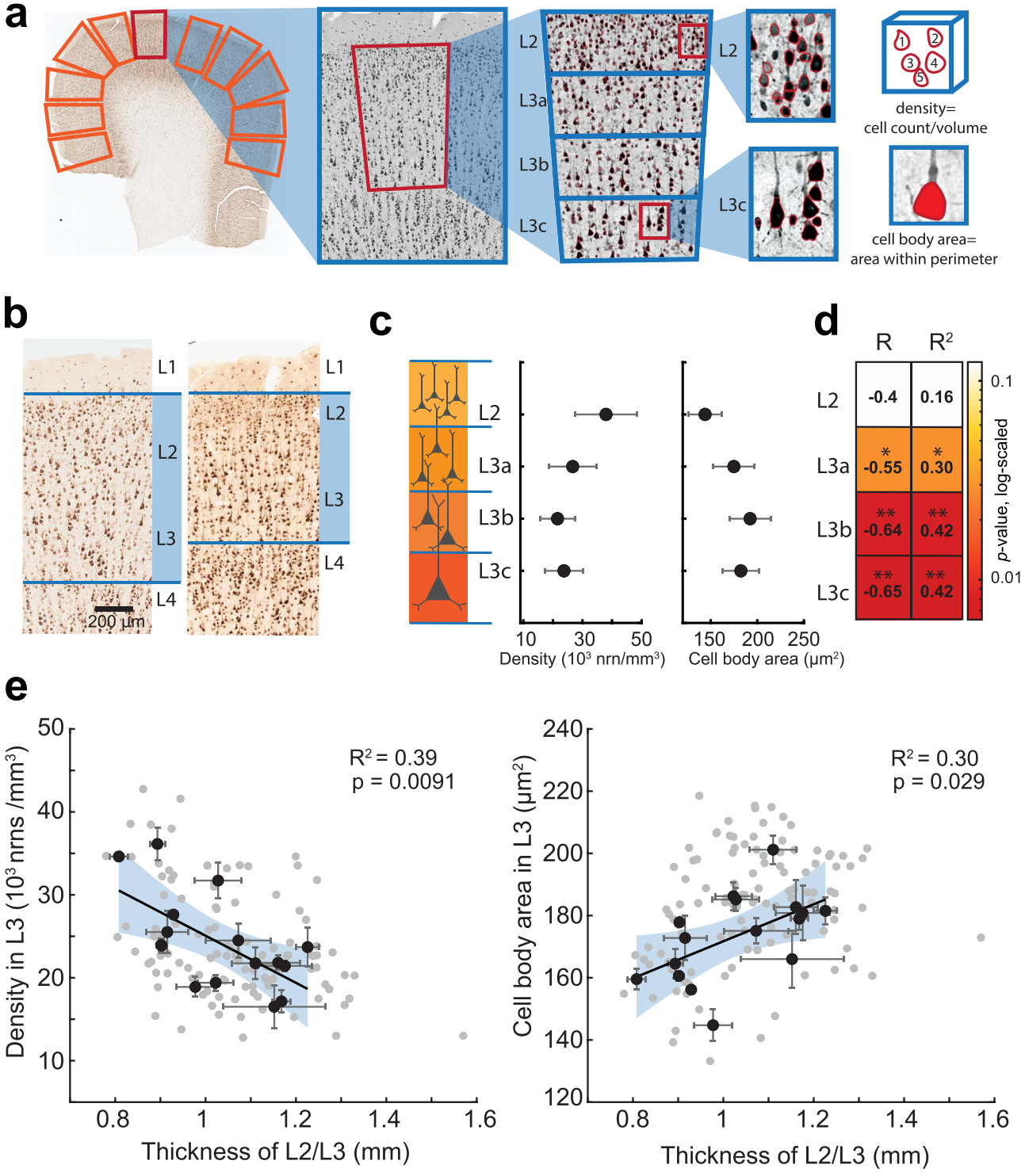

Figure 2. Thicker L2/L3 in human cortex is accompanied by lower neuronal densities and larger cell body area in layer 3. (*a*) Microstructure analysis workflow: in NeuN stained human cortical slice multiple ROIs were selected for analysis; within each ROI a region of interest was defined that included only L2/L3 and was divided in four sublayers of equal thickness (each at 25% of total L2/L3 thickness). The neurons were detected from the images using custom-made image-processing scripts (detected neurons are shown in red). (*b*) Examples of NeuN stained slices from two subjects showing different L2/L3 thickness. (*c*) Neuronal density decreases, and cell body area increases from L2 to deeper sublayers of L3 (black circles are mean data from 16 subjects; 24 slices, 113 ROIs). (*d*) Results of neuronal density correlation to L2/L3 thickness per sublayer: neuronal density correlates stronger to L2/L3 thickness in deeper layer 3: correlation coefficients (R) and variance explained (R^2) are shown per sublayer, P-values are color coded (*P-value$<$0.05; **P-value$<$0.01). (*e*) Thicker L2/3 shows negative association with neuronal density in L3 ($F(1,14) = 9.15$) and positive association with cell body area ($F(1,14) = 5.88$). black circles are means per subject, $n = 16$, gray circles are ROIs, $n = 113$, black lines are linear regression fits to subject level data, shaded area (blue) represents 95% confidence bounds.

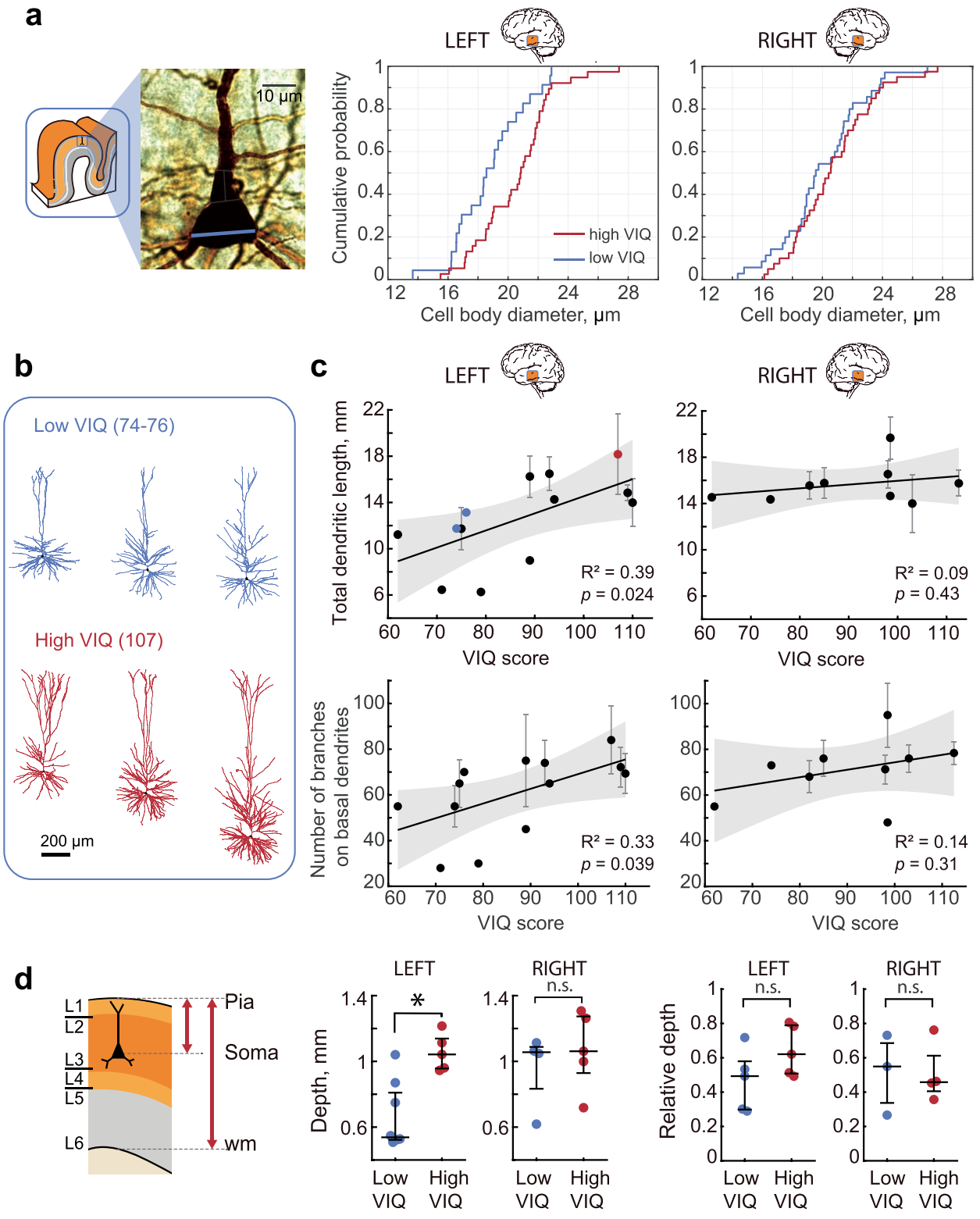

Figure 3. Pyramidal cells dendritic length associates with higher VIQ scores. (*a*) subjects with higher VIQ had larger pyramidal neurons in L2/L3: example image of a biocytin stained pyramidal neuron with soma diameter marked with blue line (left), the cumulative distribution function for all pyramidal neuron diameters in subjects with high VIQ and low VIQ for left (middle panel, *n* cells low VIQ = 23, *n* cells high VIQ = 38, Mann–Whitney *U* test: $U = 268$, $P = 0.011$) and right MTG (right panel, *n* cells low VIQ = 35, *n* cells high VIQ = 40, $U = 606$, $P = 0.32$). (*b*) Examples of fully reconstructed pyramidal neuronal morphologies (left MTG, L2/L3) from two subjects with low VIQ and one subject with high VIQ scores. (*c*) VIQ scores positively correlate with TDL (upper panel) and the number of branches (lower panel) on basal

model predictions, since AP kinetics are directly influenced by dendritic morphology, where larger dendrites lead to faster AP onsets (Eyal et al. 2014; Goriounova et al. 2018).

Discussion

Our findings point to a crucial role of supragranular layers and their pyramidal cells in human verbal cognition. These results are the first to link cortical micro-organization and cellular properties in the left MTG to a specific cognitive function this area performs—verbal intelligence. Cortical thickness and volume are among the most robust neurobiological correlates of human intelligence, and especially the left temporal cortex shows the highest correlations to general and verbal intelligence (Haier et al. 2004; McDaniel 2005; Colom et al. 2006; Choi et al. 2008; Colom et al. 2009; Karama et al. 2009; Deary et al. 2010; Basten et al. 2015), while dementia and cognitive impairment are accompanied by cortical thinning (Hof et al. 1990; Du et al. 2007). Our findings demonstrate that the overall increase in cortical thickness observed in subjects with higher intelligence can be specifically attributed to larger cortical L2/L3.

Despite the fact that our data are based on a relatively low number of subjects, the observed correlations between psychological data and cortical morpho-physiological measurements are very strong. This is due to the large interindividual differences in both intelligence scores and underlying cortical and neuronal parameters in our dataset. We limited the regional variability in cortical measurements by consistently targeting a specific cortical area in all subjects—the middle part of Brodmann area 21. Furthermore, for cortical thickness analysis, we only included gyral crowns and excluded the more variable lateral parts of the gyrus. Therefore, the observed variation in the neuronal and cortical structure and physiology most likely reflects the differences in cognitive function and not the regional differences. The variability in the cytoarchitectonic features between individuals was previously hypothesized to reflect the differences in underlying function of the area: for example, the development of language ability and differences in cytoarchitecture of Broca area (Amunts et al. 1999, 2003; Uylings et al. 2006). Similarly, differences in complexity in dendrites and spines between cortical brain areas show a gradient of complexity from primary sensory areas to higher association areas, especially in pyramidal neurons of layer 3 (Jacobs et al. 2001; Elston 2003). This gradient is thought to reflect differences in the nature of cortical processing, with spine-dense neurons at hierarchically higher association levels integrating a broader range of synaptic input than those at lower cortical levels (Jacobs et al. 2001; Elston 2003). Our data provide support to these findings by linking the complexity of dendrites to cognitive scores and showing a similar gradient in one brain area of different individuals.

The L2/L3 pyramidal cells receive rich cortico-cortical projections and have many re-excitatory connections (Shepherd 2011) that they collect on their vast dendrites. In rodents they were shown to pre-amplify information (Weiler et al. 2008) in motor cortex and induce gain modulation of deeper layer inputs in sensory cortex of rodents. This amplifying role might be even more important in multi-modal association cortices where multiple inputs have to be integrated. Deep L3 neurons have a unique pattern of dendritic maturation and have the most protracted period of developmental plasticity (Petanjek et al. 2019). They seem to be especially vulnerable and deteriorate in Alzheimer disease possibly because of their suggested role in cortico-cortical projections (Hof et al. 1990). Our findings corroborate the idea that their loss may substantially diminish the effectiveness of the distributed processing capacity of the neocortex.

Our results suggest that human higher cognitive functions are not only associated with a larger number of computational units, but rather with the size and complexity of the individual components, the neurons. We show that verbal IQ scores positively correlate with dendritic size and complexity. The longer dendrites might endow pyramidal neurons with several advantages for fast and efficient computation. Firstly, large dendrites can physically contain more synaptic contacts and process more information. Secondly, separate branches of the dendritic tree can act as independent computational compartments and increase the complexity of information processing (Poirazi et al. 2003; Gidon et al. 2020). These cells would need a larger volume to accommodate their vast dendrites, and thus spread more as the cortical volume expands leading to lower neuronal densities. Indeed, lower values of neurite density were found to be associated with higher intelligence in healthy individuals (Gençet al. 2018).

Large pyramidal neurons in layer 3 not only have extensive dendrites, they also were shown to send rich cortico-cortical projections and have an increased number and level of branching of intracortical axon projections (Kritzer and Goldman-Rakic 1995; Melchitzky and Lewis 2003). Both the increase in dendrite complexity and axonal projections might explain lower neuronal densities that we observe, and would lead to the increase in connectivity through cortical network. In humans relative to monkeys and other primates, there is a shift of the laminar origin of connections to upper layers that might result in the human brain possessing more connections with an upper layer origin (Changeux et al. 2021). Moreover, large layer 3 pyramidal neurons show a protracted dendritic and axonal maturation, that is necessary for normal cortical development, complex communication, and social abilities in children (Petanjek et al. 2019; Changeux et al. 2021). In addition, the pattern of maturation of layer 3 pyramidal neurons (dendritic development and transient increases in cell body size) coincides with the periods of rapid cognitive development and maturation during the childhood, puberty, and adolescence (Petanjek et al. 2008). This increased

dendrites from pyramidal neurons in L2/L3 in the left (n subjects = 13, n cells = 33, TDL: $F(1,11) = 6.89$, number of branches: $F(1,11) = 5.51$), but not in the right MTG (n subjects = 9, n cells = 30, TDL: $F(1,7) = 0.7$, number of branches: $F(1,7) = 1.19$). Error bars indicate SEM, shaded area (gray) represents 95% confidence bounds. The blue and red data points correspond to the examples displayed in *a*. (*d*) Cells from both groups were recorded at similar relative depths when correcting for cortical thickness Left panel: schematic showing depth of the cell as the distance from pia to soma. Relative depth was calculated as depth divided by distance from pia to white matter. Middle panel: only in the left MTG neurons recorded from subjects with higher VIQ scores were located deeper in the cortex than those from subjects with lower VIQ (Left: low VIQ Median (IQR) = 0.537(0.523–0.810) mm, n subjects = 8, n cells = 13, high VIQ = 1.042(0.957–1.139) mm, n subjects = 5, n cells = 20, $U = 38$, $P = 0.006$. Right: low VIQ = 1.056(0.833–1.088) mm, n subjects = 4, n cells = 11, high VIQ = 1.062(0.929–1.274) mm, n subjects = 5, n cells = 19, Mann–Whitney U test: $U = 18$, $P = 0.73$). Right panel: Relative depths of the recorded cells were not different (Left: low VIQ = 0.49(0.30–0.58), n subjects = 5, n cells = 9, high VIQ = 0.62(0.51–0.79), n subjects = 5, n cells = 15, $U = 21$, $P = 0.22$. Right: low VIQ = 0.55(0.34–0.69), n subjects = 3, n cells = 8, high VIQ = 0.46(0.41–0.61), n subjects = 4, n cells = 11, $U = 12$, $P = 1$). wm: white matter.

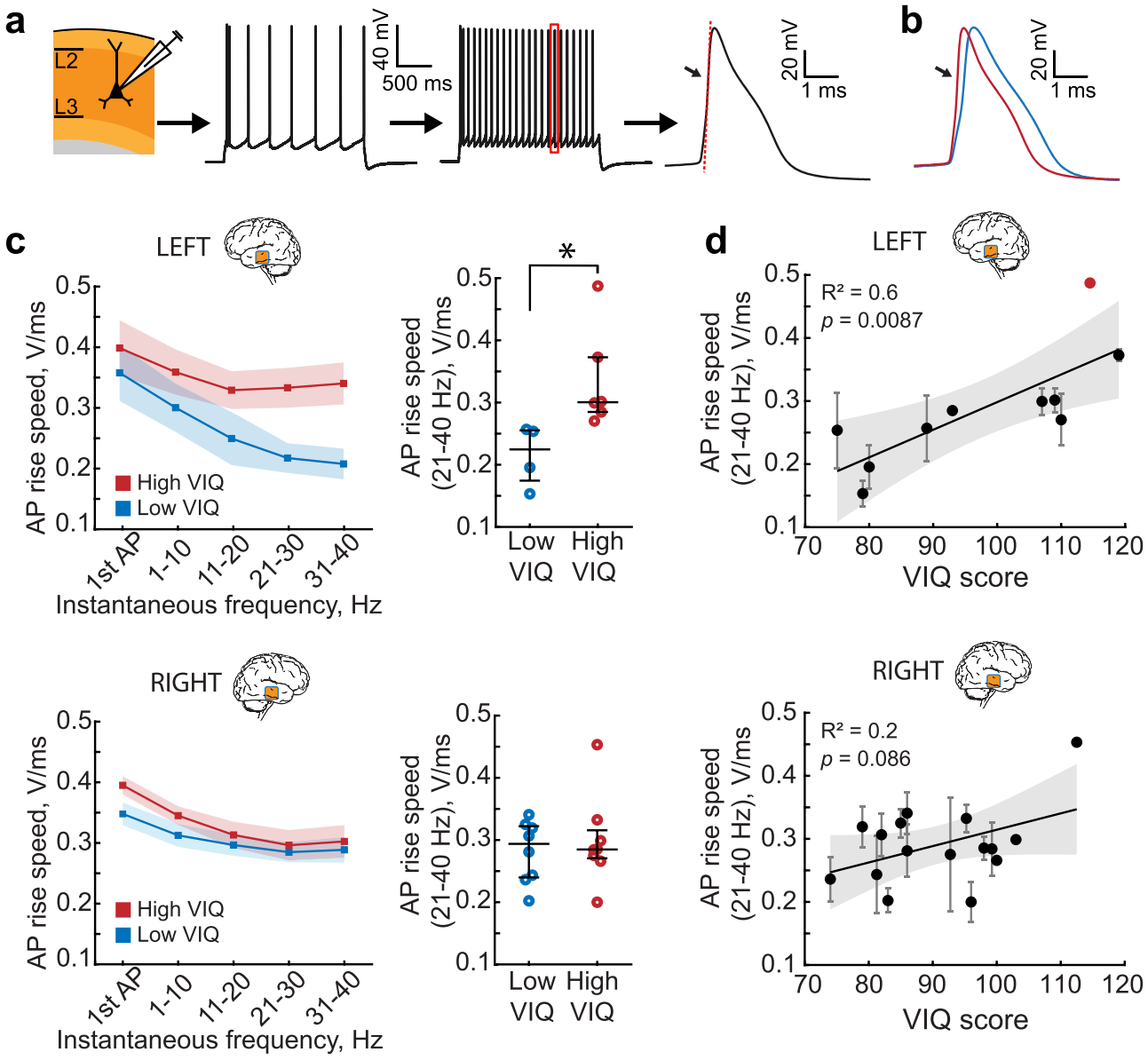

Figure 4. Left MTG pyramidal neurons in L2/L3 from subjects with higher VIQ scores are able to sustain fast action potential (AP) rise speed during high frequency firing. (*a*) AP firing in pyramidal neurons in L2/L3. AP rise speed was defined as the maximum speed of the rising phase of the AP (red dotted line). (*b*) Example AP traces at 30 Hz from two subjects with low and high VIQ. (*c*) At higher frequencies, the AP rise speed is faster in neurons from subjects with higher VIQ (red), and slower in subjects with lower VIQ (blue) only in the left MTG. Shaded area represents SEM. Each data point represents an average of APs from several per subject (Left MTG, Low VIQ Median (IQR) = 224.61(174.41–255.27) mV/ms, *n* subjects = 4, *n* cells = 15, High VIQ = 300.52(284.87–372.79) mV/ms, *n* subjects = 6, *n* cells = 16 Mann Whitney *U* test: $U = 10$, $P = 0.0095$. Right MTG, Low VIQ = 293.79(239.81–322.17) mV/msn subjects = 8, *n* cells = 36, High VIQ = 284.80(270.60–315.65) mV/ms, *n* subjects = 8, *n* cells = 29, $U = 67$, $P = 0.96$). (*d*) AP rise speeds at higher frequencies correlate with VIQ scores only in the left MTG (*n* subjects =10, *n* cells = 31, $F(1,8) = 11.9$), but not in the right MTG (*n* subjects =16, *n* cells = 65, $F(1,14) = 3.42$). After removal of the outlier (marked in red) from the analysis, the correlation remained significant ($R^2 = 0.67$, $P = 0.007$, $F(1,7) = 14.3$).

plasticity in L2/L3 network in higher order areas during cognitive development might emphasize the important role for enriched social and cultural interactions during development. Indeed, more intelligent children have a particularly plastic cortex, with an initial accelerated and prolonged phase of cortical increase (Shaw et al. 2006). Finally, the emergence of specifically human cognitive abilities in the course of evolution, including theory of mind and language, were recently speculated to be at least partially dependent on the longer maturation and fine tuning of long-range connections of upper layer neurons of the human cortex (Changeux et al. 2021).

In addition to longer dendrites, changes in the signaling speed of individual neurons must add up to increase the overall computational power of the brain. Fast signaling in the brain is a crucial requirement for efficient processing of information, and distributed brain areas of intelligence need fast signaling to coordinate their activity. Indeed, IQ scores in large groups of subjects robustly correlate with reaction times even in very simple

tasks, suggesting an underlying mental speed factor (Der and Deary 2017). Our results provide a cellular explanation for such mental speed: we show that neurons of individuals with higher verbal IQ are able to sustain action potentials with more stable fast rise times, while neurons of individuals with lower verbal IQ show neuronal "fatigue" and slowing of the AP speed. One of the computational consequence of the ability of neurons to maintain fast onsets of action potentials is the gain in temporal resolution of encoding synaptic inputs, that is, a encoding with larger bandwidth (Testa-Silva et al. 2014). In the brain, neurons are constantly bombarded by multiple incoming synaptic inputs that they need to process, filter or pass on. The ability of the neuron to resolve and react to fast-changing synaptic inputs depends on how fast it can generate APs (Goriounova et al. 2018). Thus, faster AP kinetics and better time-locking of AP output to synaptic inputs allow large pyramidal neurons to more rapidly integrate, process and convey larger amounts of synaptic information.

The firing rates of human neurons observed in vivo indicate that maintaining fast action potentials might be especially relevant during cognitive tasks. Extracellular recording in single neurons in temporal cortex during awake craniotomy for epilepsy typically show very low baseline firing rates of <1 Hz. However, during verbal tasks, such as word pair associations learning, these neurons show task-specific shifts in their levels of activity that can last for minutes (average increase of 6–9 Hz) and can increase their activity to 30–50 Hz during specific behavioral tasks (Ojemann et al. 1988, 2002; Haglund et al. 1994; Ojemann and Schoenfield-Mcneill 1998; Quian Quiroga et al. 2009). These recordings were done in the same cortical area as in our study and highlight the relevance and validity of sustained high frequency firing of MTG neurons during cognitive tasks. The ability of neurons to maintain fast kinetics of APs during such sustained firing can give them an advantage in tracking fast changing synaptic inputs.

Our dataset is a unique combination of cognitive scores, structural MRI, histological assessment and single neuron measurements, however, our method has limitations. As the cortical tissue originates from neurosurgery patients, we cannot completely rule out the influence of the disease or medication on verbal intelligence and cellular parameters. The VIQ scores from subjects in our sample are on average 90 (range 62–119), which is substantially lower than in healthy population (100). In addition, we observed an asymmetry in total cortical thickness, as well as L2/L3 thickness, with larger right MTG than the left MTG. This asymmetry reflects a natural asymmetry in cortical thickness of the middle part of the middle temporal gyrus—area of interest in this study (Kong et al. 2018). Thus, our results indicate a bidirectional association between neuronal and cortical properties: in subjects with higher intelligence L2/L3 in left MTG is thicker with larger and faster neurons, at the same time in subjects with lower intelligence the left MTG L2/L3 is thinner and contains less complex neurons with slower AP speed.

Importantly, the tissue used in this study is non-pathological, resected only to gain access to the focus of the disease. It shows no abnormalities in detailed histological examination, and we do not find any correlation of VIQ scores with any of the disease history parameters (frequency of seizures, disease duration, and disease onset, Supplementary Table 3). In addition, we and others repeatedly demonstrated that using access tissue samples, we are able to study non-pathological properties of human circuits (Molnár et al. 2008; Testa-Silva et al. 2010; Verhoog et al. 2013; Testa-Silva et al. 2014; Verhoog et al. 2016; Eyal et al. 2018; Goriounova et al. 2018; Kroon et al. 2019; Berg et al. 2021).

We emphasize the association of cortical and neuronal properties to verbal intelligence primarily based on the well-documented function of the left MTG in verbal cognition. The dominant role of the left temporal lobe in verbal ability is supported by a large body of evidence from lesion studies, semantic dementia patients, findings from studies of commissurotomy patients, and cortical mapping during awake neurosurgery (Ojemann et al. 1989; Damasio et al. 2004; Gazzaniga 2005; Binder et al. 2009). Lesions at specific locations in the left temporal lobe selectively impair specific categories of verbal reasoning such as naming of objects, tools, living things and personal names, while lesions in the right temporal lobe have much less impact on these functions (Woollams and Patterson 2018). Moreover, verbal intelligence was shown to have strong structural correlates, such as cortical thickness, exclusively in the left temporal lobe, while functional correlates seem to be more symmetrically distributed (Choi et al. 2008). Consistent with this, our findings show that the increase in cortical thickness goes hand in hand with specific changes in superficial layers of the left temporal cortex: increased layer 2 and 3 thickness, larger dendrites, larger cell body size, and decreased cell density. Furthermore, we find that variance explained (R^2) is consistently higher for linear regressions on VIQ than on PIQ. When we control for age and gender using partial correlations, the correlation coefficients for PIQ to neuronal parameters lose their statistical significance, while VIQ and FSIQ both remain high and significant (Supplementary Fig. 4). This strengthens our conclusions that the observed effects are due to the involvement of left MTG neurons in primarily verbal aspects of intelligence.

In conclusion, our results are the first to link verbal cognition with the structure of supragranular layers and their pyramidal neurons in the left temporal lobe. The findings suggest that larger size and complexity of neurons in these superficial layers might contribute to larger cortical thickness and improved human cognitive ability.

Supplementary Material

Supplementary material can be found at *Cerebral Cortex* online.

Author contributions

D.B.H.: e-phys data acquisition, data analysis, writing manuscript; R.W.: data acquisition, data analysis; A.G.: slice histology; E.H.: cell density quantification.; S.B.: layer structure analysis; S.H.: e-phys data acquisition; M.B.V.: e-phys data acquisition; E.M.: morphology data acquisition; M.L.M.: cell density quantification; S.I.: performed neurosurgery and tissue procurement; J.C.B.: performed neurosurgery and tissue procurement; P. de W.H.: performed neurosurgery and tissue procurement; M.K.: IQ data acquisition; M.M.: histology data acquisition; E.S.L.: histology data acquisition; C.P.J. de K.: morphology data acquisition and analysis; H.D.M.: study design, data analysis, writing manuscript; N.A.G.: study design, e-phys data acquisition, histology data acquisition, data analysis, writing manuscript.

Funding

Netherlands Organization for Scientific Research (NWO; VENI grant, 016.Veni.171.017 to N.A.G.); European Union's Horizon

2020 Framework Programme for Research and Innovation (Human Brain Project SGA2, 785907 and HBP SGA3, 945539 to H.D.M.); National Institute of Mental Health (U01MH114812).

Notes

Conflict of Interest: The authors declare no competing interests.

References

Amunts K, Schleicher A, Bürgel U, Mohlberg H, Uylings HB, Zilles K. 1999. Broca's region revisited: cytoarchitecture and intersubject variability. *J Comp Neurol*. 412:319–341.

Amunts K, Schleicher A, Ditterich A, Zilles K. 2003. Broca's region: Cytoarchitectonic asymmetry and developmental changes. *J Comp Neurol*. 465:72–89.

Basten U, Hilger K, Fiebach CJ. 2015. Where smart brains are different: a quantitative meta-analysis of functional and structural brain imaging studies on intelligence. *Intelligence*. 51:10–27

Berg J, Sorensen SA, Ting JT, Miller JA, Chartrand T, Buchin A, Bakken TE, Budzillo A, Dee N, Ding S-L, et al. 2021. Human neocortical expansion involves glutamatergic neuron diversification. *Nature* (in press). https://doi.org/10.1101/2020.03.31.018820.

Binder JR, Desai RH, Graves WW, Conant LL. 2009. Where is the semantic system? A critical review and meta-analysis of 120 functional neuroimaging studies. *Cereb Cortex*. 19:2767–2796.

Changeux JP, Goulas A, Hilgetag CC. 2021. A connectomic hypothesis for the hominization of the brain. *Cereb Cortex*. 31:2425–2449.

Chertkow H, Bub D, Deaudon C, Whitehead V. 1997. On the status of object concepts in aphasia. *Brain Lang*. 58:203–232.

Choi YY, Shamosh NA, Cho SH, DeYoung CG, Lee MJ, Lee J-M, Kim SI, Cho Z-H, Kim K, Gray JR, et al. 2008. Multiple bases of human intelligence revealed by cortical thickness and neural activation. *J Neurosci*. 28:10323–10329.

Coleman JRI, Bryois J, Gaspar HA, Jansen PR, Savage JE, Skene N, Plomin R, Muñoz-Manchado AB, Linnarsson S, Crawford G, et al. 2019. Biological annotation of genetic loci associated with intelligence in a meta-analysis of 87,740 individuals. *Mol Psychiatry*. 24:182–197.

Colom R, Haier RJ, Head K, Álvarez-Linera J, Quiroga MÁ, Shih PC, Jung RE. 2009. Gray matter correlates of fluid, crystallized, and spatial intelligence: testing the P-FIT model. *Intelligence*. 37:124–135.

Colom R, Jung RE, Haier RJ. 2006. Distributed brain sites for the g-factor of intelligence. *Neuroimage*. 31:1359–1365.

Damasio H, Tranel D, Grabowski T, Adolphs R, Damasio A. 2004. Neural systems behind word and concept retrieval. *Cognition*. 92:179–229.

Deary IJ, Pattie A, Starr JM. 2013. The stability of intelligence from age 11 to age 90 years: the Lothian birth cohort of 1921. *Psychol Sci*. 24:2361–2368.

Deary IJ, Penke L, Johnson W. 2010. The neuroscience of human intelligence differences. *Nat Rev Neurosci*. 11:201–211.

DeFelipe J, Alonso-Nanclares L, Arellano JI. 2002. Microstructure of the neocortex: comparative aspects. *J Neurocytol*. 31:299–316.

Der G, Deary IJ. 2017. The relationship between intelligence and reaction time varies with age: results from three representative narrow-age age cohorts at 30, 50 and 69 years. *Intelligence*. 64:89–97.

Douglas RJ, Martin KAC. 2004. Neuronal circuits of the neocortex. *Annu Rev Neurosci*. 27:419–451.

Dronkers NF, Wilkins DP, van Valin RD Jr, Redfern BB, Jaeger JJ. 2004. Lesion analysis of the brain areas involved in language comprehension. *Cognition*. 92:145–177.

Du A-T, Schuff N, Kramer JH, Rosen HJ, Gorno-Tempini ML, Rankin K, Miller BL, Weiner MW. 2007. Different regional patterns of cortical thinning in Alzheimer's disease and frontotemporal dementia. *Brain*. 130:1159–1166.

Elston GN. 2003. Cortex, cognition and the cell: new insights into the pyramidal neuron and prefrontal function. *Cereb Cortex*. 13:1124–1138.

Eyal G, Mansvelder HD, de Kock CPJ, Segev I. 2014. Dendrites impact the encoding capabilities of the axon. *J Neurosci*. 34:8063–8071.

Eyal G, Verhoog MB, Testa-Silva G, Deitcher Y, Benavides-Piccione R, DeFelipe J, de Kock CPJ, Mansvelder HD, Segev I. 2018. Human cortical pyramidal neurons: from spines to spikes via models. *Front Cell Neurosci*. 12:181.

Fischl B, van der Kouwe A, Destrieux C, Halgren E, Ségonne F, Salat DH, Busa E, Seidman LJ, Goldstein J, Kennedy D, et al. 2004. Automatically parcellating the human cerebral cortex. *Cereb Cortex*. 14:11–22.

Fischl B, Dale AM. 2000. Measuring the thickness of the human cerebral cortex from magnetic resonance images. *Proc Natl Acad Sci USA*. 97:11050–11055.

Gainotti G. 2006. Anatomical functional and cognitive determinants of semantic memory disorders. *Neurosci Biobehav Rev*. 30:577–594.

Gazzaniga MS. 2005. Forty-five years of split-brain research and still going strong. *Nat Rev Neurosci*. 6:653–659.

Genç E, Fraenz C, Schlüter C, Friedrich P, Hossiep R, Voelkle MC, Ling JM, Güntürkün O, Jung RE. 2018. Diffusion markers of dendritic density and arborization in gray matter predict differences in intelligence. *Nat Commun*. 9:1905.

Gidon A, Zolnik TA, Fidzinski P, Bolduan F, Papoutsi A, Poirazi P, Holtkamp M, Vida I, Larkum ME. 2020. Dendritic action potentials and computation in human layer 2/3 cortical neurons. *Science*. 367:83–87.

Goriounova NA, Heyer DB, Wilbers R, Verhoog MB, Giugliano M, Verbist C, Obermayer J, Kerkhofs A, Smeding H, Verberne M, et al. 2018. Large and fast human pyramidal neurons associate with intelligence. *Elife*. 7:e41714. https://doi.org/10.7554/eLife.41714.

Haglund MM, Ojemann GA, Schwartz TW, Lettich E. 1994. Neuronal activity in human lateral temporal cortex during serial retrieval from short-term memory. *J Neurosci*. 14:1507–1515.

Haier RJ, Jung RE, Yeo RA, Head K, Alkire MT. 2004. Structural brain variation and general intelligence. *Neuroimage*. 23:425–433.

Hart J, Gordon B. 1990. Delineation of single-word semantic comprehension deficits in aphasia, with anatomical correlation. *Ann Neurol*. 27:226–231.

Hillis AE, Caramazza A. 1991. Category-specific naming and comprehension impairment: a double dissociation. *Brain*. 114:2081–2094.

Hodge RD, Bakken TE, Miller JA, Smith KA, Barkan ER, Graybuck LT, Close JL, Long B, Johansen N, Penn O, et al. 2019. Conserved cell types with divergent features in human versus mouse cortex. *Nature*. 536:171–178.

Hof PR, Morrison JH, Cox K. 1990. Quantitative analysis of a vulnerable subset of pyramidal neurons in Alzheimer's disease:

I. Superior frontal and inferior temporal cortex. *J Comp Neurol*. 301:44–54.

Hutsler JJ, Lee DG, Porter KK. 2005. Comparative analysis of cortical layering and supragranular layer enlargement in rodent carnivore and primate species. *Brain Res*. 1052:71–81.

Jacobs B, Schall M, Prather M, Kapler E, Driscoll L, Baca S, Jacobs J, Ford K, Wainwright M, Treml M. 2001. Regional dendritic and spine variation in human cerebral cortex: a quantitative Golgi study. *Cereb Cortex*. 11:558–571.

Jung RE, Haier RJ. 2007. The Parieto-frontal integration theory (P-FIT) of intelligence: converging neuroimaging evidence. *Behav Brain Sci*. 30:135–154.

Kalmbach BE, Buchin A, Long B, Close J, Nandi A, Miller JA, Bakken TE, Hodge RD, Chong P, de Frates R, et al. 2018. H-channels contribute to divergent intrinsic membrane properties of Supragranular pyramidal neurons in human versus mouse cerebral cortex. *Neuron*. 100: 1194–1208.e5.

Karama S, Ad-Dab'bagh Y, Haier RJ, Deary IJ, Lyttelton OC, Lepage C, Evans AC. 2009. Positive association between cognitive ability and cortical thickness in a representative US sample of healthy 6 to 18 year-olds. *Intelligence*. 37:145–155.

Kong X-Z, Mathias SR, Guadalupe T, Group ELW, Glahn DC, Franke B, Crivello F, Tzourio-Mazoyer N, Fisher SE, Thompson PM, et al. 2018. Mapping cortical brain asymmetry in 17,141 healthy individuals worldwide via the ENIGMA consortium. *Proc Natl Acad Sci USA*. 115:E5154–E5163.

Kritzer MF, Goldman-Rakic PS. 1995. Intrinsic circuit organization of the major layers and sublayers of the dorsolateral prefrontal cortex in the rhesus monkey. *J Comp Neurol*. 359:131–143.

Kroon T, Dawitz J, Kramvis I, Anink J, Obermayer J, Verhoog MB, Wilbers R, Goriounova NA, Idema S, Baayen JC, et al. 2019. Group I mGluR-mediated activation of Martinotti cells inhibits local cortical circuitry in human cortex. *Front Cell Neurosci*. 13:315.

McDaniel M. 2005. Big-brained people are smarter: a meta-analysis of the relationship between in vivo brain volume and intelligence. *Intelligence*. 33:337–346.

Melchitzky DS, Lewis DA. 2003. Pyramidal neuron local axon terminals in monkey prefrontal cortex: differential targeting of subclasses of GABA neurons. *Cereb Cortex*. 13:452–460.

Mohan H, Verhoog MB, Doreswamy KK, Eyal G, Aardse R, Lodder BN, Goriounova NA, Asamoah B, Brakspear ABCB, Groot C, et al. 2015. Dendritic and axonal architecture of individual pyramidal neurons across layers of adult human neocortex. *Cereb Cortex*. 25:4839–4853.

Molnár G, Olah S, Komlósi G, Füle M, Szabadics J, Varga C, Barzo P, Tamas G. 2008. Complex events initiated by individual spikes in the human cerebral cortex. *PLoS Biol*. 6: e222.

Obermayer J, Heistek TS, Kerkhofs A, Goriounova NA, Kroon T, Baayen JC, Idema S, Testa-Silva G, Couey JJ, Mansvelder HD. 2018. Lateral inhibition by Martinotti interneurons is facilitated by cholinergic inputs in human and mouse neocortex. *Nat Commun*. 9:4101–4114.

Ojemann G, Ojemann J, Lettich E, Berger M. 1989. Cortical language localization in left, dominant hemisphere. An electrical stimulation mapping investigation in 117 patients. *J Neurosurg*. 71:316–326.

Ojemann GA, Creutzfeldt O, Lettich E, Haglund MM. 1988. Neuronal activity in human lateral temporal cortex related to short-term verbal memory, naming and reading. *Brain*. 111:1383–1403.

Ojemann GA, Schoenfield-Mcneill J. 1998. Neurons in human temporal cortex active with verbal associative learning. *Brain Lang*. 64:317–327.

Ojemann GA, Schoenfield-McNeill J, Corina DP. 2002. Anatomic subdivisions in human temporal cortical neuronal activity related to recent verbal memory. *Nat Neurosci*. 5:64–71.

Patel Y, Parker N, Shin J, Howard D, French L, Thomopoulos SI, Pozzi E, Abe Y, Abé C, Anticevic A, et al. 2021. Virtual histology of cortical thickness and shared neurobiology in 6 psychiatric disorders. *JAMA Psychiat*. 78:47–63.

Petanjek Z, Judas M, Kostović I, Uylings HBM. 2008. Lifespan alterations of basal dendritic trees of pyramidal neurons in the human prefrontal cortex: a layer-specific pattern. *Cereb Cortex*. 18:915–929.

Petanjek Z, Sedmak D, Džaja D, Hladnik A, Rašin MR, Jovanov-Milosevic N. 2019. The protracted maturation of associative layer IIIC pyramidal neurons in the human prefrontal cortex during childhood: a major role in cognitive development and selective alteration in autism. *Front Psych*. 10:122. https://doi.org/10.3389/fpsyt.2019.00122.

Poirazi P, Brannon T, Mel BW. 2003. Pyramidal neuron as two-layer neural network. *Neuron*. 37:989–999.

Quian Quiroga R, Kraskov A, Koch C, Fried I. 2009. Explicit encoding of multimodal percepts by single neurons in the human brain. *Curr Biol*. 19:1308–1313.

Self MW, van Kerkoerle T, Goebel R, Roelfsema PR. 2019. Benchmarking laminar fMRI: neuronal spiking and synaptic activity during top-down and bottom-up processing in the different layers of cortex. *Neuroimage*. 197:806–817.

Shaw P, Greenstein D, Lerch J, Clasen L, Lenroot R, Gogtay N, Evans A, Rapoport J, Giedd J. 2006. Intellectual ability and cortical development in children and adolescents. *Nature*. 440:676–679.

Shepherd GM. 2011. The microcircuit concept applied to cortical evolution: from three-layer to six-layer cortex. *Front Neuroanat*. 5:30.

Strenze T. 2007. Intelligence and socioeconomic success: a meta-analytic review of longitudinal research. *Intelligence*. 35:401–426.

Testa-Silva G, Verhoog MB, Goriounova NA, Loebel A, Hjorth J, Baayen JC, de Kock CPJ, Mansvelder HD. 2010. Human synapses show a wide temporal window for spike-timing-dependent plasticity. *Front Synaptic Neurosci*. 2:12.

Testa-Silva G, Verhoog MB, Linaro D, de Kock CPJ, Baayen JC, Meredith RM, De Zeeuw CI, Giugliano M, Mansvelder HD. 2014. High bandwidth synaptic communication and frequency tracking in human neocortex. *PLoS Biol*. 12:e1002007.

Uylings HBM, Jacobsen AM, Zilles K, Amunts K. 2006. Left-right asymmetry in volume and number of neurons in adult Broca's area. *Cortex*. 42:652–658.

Uylings HBM, Rajkowska G, Sanz-Arigita E, Amunts K, Zilles K. 2005. Consequences of large interindividual variability for human brain atlases: converging macroscopical imaging and microscopical neuroanatomy. *Anat Embryol*. 210:423–431.

Verhoog MB, Goriounova NA, Obermayer J, Stroeder J, Hjorth JJJ, Testa-Silva G, Baayen JC, de Kock CPJ, Meredith RM, Mansvelder HD. 2013. Mechanisms underlying the rules for associative plasticity at adult human neocortical synapses. *J Neurosci*. 33:17197–17208.

Verhoog MB, Obermayer J, Kortleven CA, Wilbers R, Wester J, Baayen JC, de Kock CPJ, Meredith RM, Mansvelder HD. 2016.

Layer-specific cholinergic control of human and mouse cortical synaptic plasticity. *Nat Commun*. 7:12826.

Wang B, Yin L, Zou X, Ye M, Liu Y, He T, Deng S, Jiang Y, Zheng R, Wang Y, et al. 2015. A subtype of inhibitory interneuron with intrinsic persistent activity in human and monkey neocortex. *Cell Rep*. 10:1450–1458.

Weiler N, Wood L, Yu J, Solla SA, Shepherd GMG. 2008. Top-down laminar organization of the excitatory network in motor cortex. *Nat Neurosci*. 11:360–366.

Woollams AM, Patterson K. 2018. Cognitive consequences of the left-right asymmetry of atrophy in semantic dementia. *Cortex*. 107:64–77.